Studying arrhythmogenic right ventricular dysplasia with patient-specific iPSCs

Changsung Kim[1], **Johnson Wong**[1], **Jianyan Wen**[1,4], **Shirong Wang**[1], **Cheng Wang**[1], **Sean Spiering**[2], **Natalia G. Kan**[2], **Sonia Forcales**[2], **Pier Lorenzo Puri**[2], **Teresa C. Leone**[3], **Joseph E. Marine**[5], **Hugh Calkins**[5], **Daniel P. Kelly**[3], **Daniel P. Judge**[5], and **Huei-Sheng Vincent Chen**[1,6]

[1]Del E. Webb Center for Neuroscience, Aging & Stem Cell Research, La Jolla, California 92037 and Orlando, Florida 32827, USA

[2]Muscle Regeneration and Development Program, La Jolla, California 92037 and Orlando, Florida 32827, USA

[3]Diabetes and Obesity Research Center, Sanford-Burnham Medical Research Institute, La Jolla, California 92037 and Orlando, Florida 32827, USA

[4]Department of Cardiovascular Surgery, China-Japan Friendship Hospital, Beijing 100029, China

[5]Department of Medicine/Cardiology, Johns Hopkins University School of Medicine, Baltimore, Maryland 21287, USA

[6]Department of Medicine/Cardiology, University of California-San Diego, San Diego, California, 92103, USA

Abstract

Cellular reprogramming of somatic cells to patient-specific induced pluripotent stem cells (iPSCs) enables *in-vitro* modelling of human genetic disorders for pathogenic investigations and therapeutic screens[1–7]. However, using iPSC-derived cardiomyocytes (iPSC-CMs) to model an adult-onset heart disease remains challenging due to the uncertainty regarding the ability of relatively immature iPSC-CMs to fully recapitulate adult disease phenotypes. Arrhythmogenic right ventricular dysplasia/cardiomyopathy (ARVD/C) is an inherited heart disease characterized by pathological fatty infiltration and cardiomyocyte loss predominantly in the right ventricle (RV)[8], which is associated with life-threatening ventricular arrhythmias. Over 50% of affected individuals have desmosome gene mutations, most commonly in *PKP2* encoding plakophilin-2[9].

Correspondence and requests for materials should be addressed to H.-S. Vincent Chen, M.D., Ph.D., Sanford-Burnham Medical Research Institute, 10901 North Torrey Pines Road, La Jolla, California 92037, USA. Tel: 858-646-3183; Fax: 858-795-5273 (hsv_chen@burnham.org).

The median age at presentation of ARVD/C is 26 years[8]. We used Yamanaka's methods[1,10] to generate iPSC lines from fibroblasts of two patients with ARVD/C and *PKP2* mutations[11,12]. Mutant *PKP2* iPSC-CMs demonstrate abnormal plakoglobin nuclear translocation and decreased β-catenin activity[13] in cardiogenic conditions; yet these abnormal features are insufficient to reproduce the pathological phenotypes of ARVD/C in standard cardiogenic conditions. Here we show that induction of adult-like metabolic energetics from an embryonic/glycolytic state and abnormal peroxisome proliferator-activated receptor-gamma (PPARγ) activation underlie the pathogenesis of ARVD/C. By coactivating normal PPAR-alpha (PPARα)-dependent metabolism and abnormal PPARγ pathway in beating embryoid bodies (EBs) with defined media, we established an efficient ARVD/C *in-vitro* model within two months. This model manifests exaggerated lipogenesis and apoptosis in mutant *PKP2* iPSC-CMs. iPSC-CMs with a homozygous *PKP2* mutation also displayed calcium-handling deficits. Our study is the first to demonstrate that induction of adult-like metabolism plays a critical role in establishing an adult-onset disease model using patient-specific iPSCs. Using this model, we revealed crucial pathogenic insights that metabolic derangement in adult-like metabolic milieu underlies ARVD/C pathologies, enabling us to propose novel disease-modifying therapeutic strategies.

Mutations resulting in ARVD/C are frequently found in five components of the cardiac desmosome, which include junction plakoglobin, plakophilin-2 (Pkp2), desmoplakin (Dsp), desmoglein-2, and desmocollin-2[9]. Pathological hallmarks of ARVD/C are progressive fibro-fatty replacement of cardiomyocytes with increased cardiomyocyte apoptosis primarily in the RV. Pathogenic processes of ARVD/C are difficult to study because 1) obtaining cardiac samples from early stages of human ARVD/C hearts is not possible due to ARVD/C being commonly diagnosed at advance diseased stages or post-mortem[8], and 2) primary cardiac tissues are difficult to biopsy safely from symptomatic ARVD/C patients due to the risk of cardiac perforation. Moreover, mouse models of ARVD/C remain unproven for finding clinically feasible therapy. These limiting factors impose significant constraints in developing therapies for human ARVD/C.

Using four retroviral vectors containing *Oct4, Sox2, Klf4,* and *cMyc*, we first generated several iPSC lines from fibroblasts of a patient with clinical ARVD/C and a homozygous c.2484C>T mutation in *PKP2* that causes cryptic splicing with a 7-nucleotide deletion in exon 12, leading to frame-shift of the C-terminal proteins[11]. Three iPSC lines were extensively characterized: JK#2, JK#7, and JK#11 (Fig. 1 and Supplementary Figs. 1–2). All iPSC clones expressed pluripotent markers including *Oct4, Tra1-81, Nanog*, and *SSEA4*; displayed normal karyotypes; and formed teratoma when injected into severe combined immunodeficient (SCID) mice. Pluripotent status of mutant *PKP2*-iPSCs was also demonstrated by the methylation patterns of *Nanog* promoter regions (Fig. 1c) in comparison to parental mutant *PKP2* fibroblasts and H9 human embryonic stem cells (hESCs). Global transcriptome expression profiles showed that all mutant *PKP2*-iPSC lines depicted a higher degree of similarity with H9 hESCs and normal iPSCs (CF-iPSCs, female, characterized in Supplementary Fig. 3) than their parental fibroblasts (Fig. 1f). Importantly, all three JK mutant iPSC lines showed silenced exogenous retroviral transgenes and activation of endogenous pluripotent genes (Supplementary Fig. 2). Genomic DNA sequencing and mRNA analysis confirmed the homozygous c.2484C>T mutation in *PKP2*

that caused predominantly cryptic splicing in exon 12 of three JK lines (Supplementary Fig. 1d & 2b). These results demonstrated the successful reprogramming of parental mutant *PKP2* fibroblasts to iPSC lines.

We differentiated human H9 hESCs, CF-iPSCs, and mutant *PKP2*-iPSCs to beating EBs (Supplementary Videos 1–2) using a standard cardiogenic protocol[14]. Consistent with previous findings in ARVD/C cell line and mouse models with desmoplakin downregulation/deletion[13], we observed abnormal nuclear translocation of junction plakoglobin proteins (Pkg) (Fig. 2a–b), and very low β-catenin activity and expression in mutant iPSC-CMs (Supplementary Fig. 4) but not in normal hESC-CMs under baseline cardiogenic conditions. These results indicate that mutant Pkp2 proteins with frame-shifted C-terminals fail to anchor Pkg to the sarcolemmal membrane, resulting in Pkg nuclear translocation and downregulation of β-catenin activities[13]. However, no exaggerated lipogenesis (by Nile Red staining) or apoptosis (by TUNEL assay) in H9 hESC- or mutant iPSC-CMs was found after culturing for 2–3 months in this baseline cardiogenic condition (Fig. 2c), an observation that is consistent with the delayed, adult-onset clinical course of ARVD/C.

We then focused our studies on the cardiomyocyte portions [positive for cardiac αActinin or troponin I (cTnI)] of beating EBs. We counted 1) the percentage of cardiomyocytes that possessed positive TUNEL nuclear staining as the cardiomyocyte (CM) apoptotic index, and 2) the percentage of cardiomyocytes that contained any Nile Red-positive lipid droplets as the indicator of lipogenesis in cardiomyocytes. The baseline apoptotic index and percentages of lipid-laden cardiomyocytes are 1.8±0.3 & 0.8±0.5 % for 60 day-old (60D) hESC-CMs, and 2.1±0.6 & 0.9±0.1% for 60D mutant *PKP2* iPSC-CMs (no statistical difference between these two groups), respectively. Since the major metabolic differences between embryonic and adult cardiomyocytes are 1) embryonic cardiomyocytes use mostly glycolysis for energy production, and 2) adult cardiomyocytes produce most energy via fatty acid oxidation (FAO) but retain capacity to readily switch to glucose or other substrate utilization when fatty acid is not available or FAO is compromised[15,16], we first created a lipogenic milieu in beating EBs with an adipogenic cocktail [insulin, dexamethasone, and 3-isobutyl-1-methilxanthine (IBMX), termed the 3-factor (3F) protocol][17–19] in an attempt to induce adult-like energy metabolism and accelerate pathogenesis in mutant iPSC-CMs. With this 3F protocol, we observed mildly increased lipogenesis with minimal apoptosis after 4–5 weeks of treatment (13.2±4.3 & 4.8±1.0% lipid-laden cardiomyocytes and 6.3±1.4 & 3.9±1.8% apoptotic cardiomyocytes in hESC-CMs and mutant *PKP2* iPSC-CMs, respectively, *p=NS* between groups, Fig. 2d–k). Notably, this 3F protocol induced more expression of PPAR-alpha (PPARα), the major transcriptional regulator of fatty acid metabolism in adult cardiomyocytes[16], in beating mutant iPSC-EBs than hESC-EBs (Fig. 2g). PPARγ, which should be minimally activated in normal cardiomyocytes, was slightly activated by this 3F protocol in both beating EBs. Because PPARγ pathway has been reported to be abnormally hyperactivated in RV tissue samples of ARVD/C hearts[20] and transgene-induced over-expression of PPARγ in mouse cardiomyocytes leads to dilated cardiomyopathy[21], we added 5 μM rosiglitazone[22] and 200 μM indomethacin[23] to the 3F protocol to further induce abnormal PPARγ over-activation in beating EBs [termed the 5-

factor (5F) protocol]. After 4–5 weeks of treatment with 5F, mutant iPSC-CMs demonstrated exaggerated lipogenesis ($31.6\pm3.3\%$ versus 13.5 ± 3.5 % in hESC-CMs, $p<0.05$) and pronounced apoptosis ($39.6\pm8.5\%$ versus 5.4 ± 0.9 % in hESC-CMs, $p<0.05$, Fig. 2h–k). Quantitative RT-PCR (qRT-PCR) analysis also confirmed the higher expression of adipogenic PPARγ/aP2 (fatty acid–binding protein) genes and downregulation of the pro-survival Bcl2 gene in beating mutant *PKP2*-EBs when compared to normal hESC-EBs or CF-iPSC-EBs (Fig. 2g and Supplementary Fig. 5a–b). Results of cardiomyocytes apoptosis and lipogenesis in beating EBs after control, 3F, or 5F treatment are summarized in Figs. 2j–k. We also observed abnormal PPARγ nuclear staining in mutant *PKP2* iPSC-CMs after 2 weeks of 5F treatment (Supplementary Fig. 5c), indicating abnormal PPARγ activation may play a significant role in mediating mutant iPSC-CM pathology. We previously showed that we could use cardiac alpha-myosin heavy chain promoter-driven Puromycin resistance (αMHC-Puro^r) to efficiently isolate cardiomyocytes (>95% purity) from beating EBs[14]. We therefore generated mutant iPSC lines (JK#2 & #11) with αMHC-Puro^r to enable purification of cardiomyocytes for further testing. In comparison to Puromycin-isolated hESC-CMs, purified mutant iPSC-CMs showed higher PPARγ activation, lower Bcl2, and higher apoptotic caspase 3 expressions after 5F treatment (Supplementary Fig. 5d). More importantly, rosiglitazone and indomethacin alone without the other three factors induced PPARγ activation only but did not induce exaggerated lipogenesis or apoptosis (Supplementary Fig. 5e–g), indicating that activation of both normal PPARα and abnormal PPARγ pathways in mutant *PKP2* iPSC-CMs is required for eliciting pathologies of ARVD/C.

We further verified that the pathogenic specificity of these ARVD/C phenotypes is due to the *PKP2* mutation in mutant iPSC-EBs by introducing the wild-type (WT) *PKP2* gene back into mutant iPSC-CMs, containing αMHC-Puro^r, with a lentiviral transduction method (Fig. 3a). After transducing beating mutant iPSC-EBs with WT *PKP2* [verified by the expression of tagged green fluorescent protein (GFP)], abnormal Pkg nuclear localization (Fig. 3b), apoptosis (Fig. 3c), and lipogenesis (Fig. 3d) in Puromycin-purified mutant iPSC-CMs were corrected by the expression of WT *PKP2* (GFP+) but not in isolated CMs without WT-*PKP2*-GFP after the 5F protocol. We measured the number of lipid droplets in each cardiomyocyte as the degree of lipogenesis in Fig. 3d because cardiomyocytes containing WT-*PKP2*-GFP still had few tiny lipid droplets remaining after 5F treatment (Fig. 3d, left image). Also, control GFP vector alone without WT-*PKP2* did not correct the Pkg nuclear translocation (Fig. 3b) or the large number of big lipid droplets found in mutant *PKP2* iPSC-CMs (Fig. 3d, right image) after pathogenic induction. These findings support that observed pathological phenotypes are the result of mutated *PKP2* genes in iPSCs.

Among the components of pathogenic 5F protocol, insulin, dexamethasone, and IBMX simulate natural hormonal regulation of cardiomyocyte metabolism, but rosiglitazone and indomethacinare not natural human ligands. Therefore, we searched for a natural ligand that could replace rosiglitazone and indomethacin for inducing abnormal PPARγ activation. We found that the endogenous PPARγ activator 13-hydroxyocta-decadienoic acid [13-HODE, a major component of the oxidized low-density lipoprotein (oxLDL)][22] could replace rosiglitazone and indomethacin in the 5F protocol for abnormal PPARγ activation, leading

to extensive lipogenesis (37.5±6.0%) and apoptosis (22.4±4.0%) in mutant iPSC-CMs (Fig. 3e). Moreover, in order to support the crucial pathogenic role of coactivation of abnormal PPARγ and normal PPARα pathways in ARVD/C, we showed that blockade of PPARγ overactivation with PPARγ antagonists, GW9662 (GW)[22] or T0070907 (T007)[23], during pathogenic induction with media containing 13-HODE and 3-factors, prevents apoptosis and lipogenesis in mutant iPSC-CMs (Fig. 3f–h). Also, blockade of PPARα activation with an antagonist, 2 μM GW6471 after 5F treatment (Supplementary Fig. 6) or activation of PPARγ alone (Supplementary Fig. 5e–g) did not induce significant ARVD/C pathologies, supporting the crucial role of PPARα/PPARγ coactivation in ARVD/C pathogenesis. Significant FAO and β-oxidation activated by PPARα appear to be required for cardiomyocyte apoptosis as well (Supplementary Fig. 6b–e). Furthermore, because mitochondrial function is tightly linked to energy metabolism and apoptosis[24], we decreased reactive oxygen species (ROS) production from mitochondria with ROS scavengers, 1 mM N-acetyl-cysteine or ascorbic acid individually, in the 5F pathogenic protocol, which markedly decreased cardiomyocyte death in mutant *PKP2*-beating EBs (Fig. 3i–j).

Using the Seahorse XF96 Extracellular Flux Analyzer[25], functional assays of FAO and glycolysis in live cells revealed that mutant *PKP2* iPSC-CMs and normal iPSC-CMs derived from a second normal iPSC line (hS-iPSC, male, characterized in Supplementary Fig. 7) had dominant glycolytic energetics (an embryonic pattern[15]) at the baseline (Fig. 4 and Supplementary Fig. 8). After activation of PPARα by 3F, mutant and normal iPSC-CMs displayed similar levels of glycolysis but significant activation of FAO (an adult-like pattern) when compared to the un-induced, baseline conditions (zero factor). Compared to 3F induction, mutant *PKP2* iPSC-CMs after pathogenic coactivation of PPARα and PPARγ by 5F demonstrated overall depressed energy metabolism with 86% reduction in FAO and 74% reduction in glycolysis, resulting in a fuel shift from using both fatty acids and glucose to dominant glucose utilization (including glycolysis and pyruvate oxidation), much like the so-called metabolic burnt-out state observed in failing hearts[26] (Fig. 4). This fuel-shift after pathogenic induction is accompanied by significant downregulation of mRNA transcripts of carnitine palmitoyltransferase-1B (CPT-1B) and pyruvate dehydrogenase kinase-4 (PDK4), leading to inhibition of FAO and activation of pyruvate dehydrogenase (PDH) for increased pyruvate oxidation[16,26], respectively (Fig. 4i–k). Thus, results from immunocytochemical, genetic, and metabolic assays support strongly that coactivation of PPARα and PPARγ by hormones and small molecules accelerates the pathogenesis and establishes an efficient *in-vitro* model of ARVD/C, recapitulating the metabolic and pathological signatures of failing ARVD/C hearts within two months.

We also used Yamanaka's episomal method[10] to generate three lines of genome-integration free iPSC (SW#5, 6, and 7) from a second patient with clinical ARVD/C (Supplementary Fig. 9) and a heterozygous c.2013delC in exon 10 of *PKP2* (termed delC *PKP2* mutation) that causes frame-shift and premature termination in exon10. Confirmation of pluripotent status and the heterozygous c.2013delC in *PKP2* of these three SW iPSC clones are shown in Supplementary Figs. 10–11. Prematurely-terminated delC mutant *PKP2* transcripts are likely unstable and degraded to undetectable levels (see Supplementary Fig. 10b–c and Fig. 11h). SW iPSC-CMs also showed increased nuclear Pkg translocation (Supplementary Fig.

12a–c) and very low β-catenin nuclear localization (Supplementary Fig. 4) as described for the homozygous c.2484C>T mutant *PKP2* iPSC-CMs. We induced ARVD phenotypes from SW#5 and #7 mutant iPSC-CMs but not in normal female CF-iPSC-CMs with the 5F protocol. Only the 5F protocol induced coactivation of normal PPARα and abnormal PPARγ pathways that led to exaggerated lipogenesis and cardiomyocyte apoptosis in delC *PKP2* iPSC-CMs (Supplementary Fig. 12), consistent with the results shown in Fig. 2. The second hS-iPSC line was also used to show that 5F protocol did not induce exaggerated lipogenesis or cardiomyocyte apoptosis in normal male iPSC-CMs (Supplementary Fig. 7f).

We further used JK mutant iPSC-CMs to investigate other cardiomyocyte properties that may contribute to pathogenesis. Compared to H9 hESC-CMs in baseline conditions, mutant iPSC-CMs demonstrated slower intracellular calcium ($[Ca^{2+}]_i$) relaxation after pacing only in high extracellular Ca^{2+} media (5.8 mM) with a prolonged relaxation time constant but not in normal Ca^{2+} media (1.8 mM). However, after 5F pathogenic induction, mutant iPSC-CMs demonstrated a prolonged $[Ca^{2+}]_i$ relaxation phase even in normal Ca^{2+} media after pacing (Supplementary Fig. 13a–d), indicating abnormal $[Ca^{2+}]_i$ handling capability. Furthermore, using Puromycin-purified cardiomyocytes and compared to hESC-CMs, qRT-PCR analysis of mutant iPSC-CMs in baseline conditions showed mildly decreased expression levels of sarcoplasmic reticulum Ca^{2+}-ATPase (SERCA, for Ca^{2+} re-uptake) with preserved Na^+/Ca^{2+} exchanger 1 (NCX1, for $[Ca^{2+}]_i$ extrusion) expression, which may explain the impaired $[Ca^{2+}]_i$ relaxation of mutant iPSC-CMs only in high extracellular Ca^{2+} media at baseline. In contrast, after 5F treatment, both NCX1 and SERCA expression levels were significantly downregulated (Supplementary Fig. 13e–f) relative to hESC-CMs, which would account for the further impaired $[Ca^{2+}]_i$ relaxation phase of mutant iPSC-CMs even in normal Ca^{2+} media. Also, electrophysiological properties of JK *PKP2* mutant iPSC-CMs are different from H9 hESC-CMs (Supplementary Fig. 14) at baseline and show further impairment after PPARα and PPARγ coactivation. Future mechanistic studies are needed to determine the roles of impaired $[Ca^{2+}]_i$ handling and altered electrical properties in mediating pathologies or arrhythmia of mutant iPSC-CMs[8,27].

Finally, in order to explain the predominant pathology in RV of ARVD/C hearts, we increased the number of Islet l-positive (Isl1+) cardiac progenitor cells by ~ 4-fold in JK#2 & #11 mutant *PKP2* iPSCs with 1μM 6-bromoindirubin-3′-oxime (BIO)[28] to simulate natural RV formation from Isl1+ progenitor cells of the secondary heart field[29] (Supplementary Fig. 15a–c). We also used 100 ng/ml Dickkopf-1 (Dkk1)[28] to decrease the number of Isl1+ progenitor cells and, subsequently, RV-like cardiomyocytes. After 5F pathogenic induction, EBs with enriched Isl1+ cells had significantly more lipogenesis and apoptosis in cardiomyocytes than EBs with minimal numbers of Isl1+ progenitor cells (Supplementary Fig. 15d–g). This result supports the notion that Isl1+ cells confer the dominant pathologies in the RV[30].

In conclusion, using patient-specific mutant *PKP2*-iPSCs and various pathogenic conditions, we accelerate the pathogenesis of an adult-onset disease. We demonstrate the importance of PPARα/PPARγ coactivation, ROS production, fatty acid oxidation and Isl1+ cells in the pathogenesis of ARVD/C. These efficient *in-vitro* iPSC models recapitulate the

pathognomonic features of ARVD/C and enable pathogenic investigation and therapeutic screens.

Methods

Culture conditions and generation of PKP2 iPSCs

We obtained normal and mutant *PKP2* human fibroblasts from University of California-San Diego and Johns Hopkins University after informed consent was obtained from all subjects under approved study protocols by respective Institutional Review Boards at both universities and SBMRI. The clinical presentation, diagnostic data, and genetic analysis of the first patient and her family members were published previously[11]. Normal fibroblasts were obtained from discarded heart and skin of aborted foetuses of pregnant females without ARVD/C and any family history of ARVD/C. HEK 293T cells and human fibroblasts were cultured in Dulbecco's Modified Eagle Media (DMEM, Hyclone) containing 10% heat-inactivated fetal bovine serum (FBS), 1 mM non-essential amino acids (NEAAs), 1x GlutaMAX, and 100 unit/ml penicillin with 100 μg/ml streptomycin (penicillin/streptomycin). Human iPSCs and H9 hESCs were cultured on irradiated mouse embryonic fibroblast (MEF) feeders in stem cell media containing Knockout (KO)-DMEM, 20% KO Serum Replacement (SR), 1 mM NEAAs, 1x GlutaMAX, 0.1 mM β-mercaptoethanol, penicillin/streptomycin, and 8 ng/mlbFGF (Sigma). Retroviral plasmids, pMXs-hc-MYC, pMXs-hSOX2, pMXs-hKLF4, and pMXs-hOCT3/4, were purchased from Addgene (MA, USA). The protocol to generate iPSC lines with retroviral plasmids is essentially the same as previously published by Yamanaka's group[1]. Briefly, each pMXs retroviral vector along with pMs-gag/pol and PCMV-VSV-G plasmids at the ratio of 2:2:1 (total 20 μg) were cotransfected to HEK-293T cells for viral particle production. At 36 hours after transfection, DMEM containing viruses from each plate were collected, mixed with 8 μg/ml polybrene (Sigma), and immediately used to infect human fibroblasts (100,000 cells) by spinning transduction. Six days after the first infection, a half-million infected fibroblasts were trypsinized and plated on 100 mm dishes containing irradiated MEF feeder layers in 10% FBS-containing DMEM. One day later, the media was changed to stem cell media as described above. Induced pluripotent colonies were selected based on stem cell-like morphologies at 12–14 days after the initial infection. All culture media and reagents were purchased from Invitrogen (Carlsbad, CA) unless indicated otherwise.

The episomal method of generating integration-free iPSC colonies is the same as published by Yamanaka's group using pCXLE-EGFP, pCXLE-hOCT3/4-shp53-F, pCXLE-hSK, and pCXLE-hUL (Addgene) episomal vectors[10].

Cardiomyocyte differentiation

Our standard cardiogenic protocol to produce beating EBs was published previously[14] and the cardiogenic media was EB media: KO-DMEM with 20% FBS, 1 mM NEAAs, 1x GlutaMAX, 1 mM β-mercaptoethanol, and penicillin/streptomycin. A modified Keller's method[31] to enrich cardiac progenitor cells was also used and optimized for our hESCs and iPSCs. After beating EBs were observed, they were maintained in the EB media containing

only 2% FBS. The method to purify cardiomyocyte spheroids (CSs) from EBs containing αMHC-Puro[r] was published previously[14, 32].

Adipogenic conditions and pharmacological investigation

In the presence of very low serum concentrations (2% FBS), we used low micromolar concentrations of insulin (50 μg/ml) and dexamethasone (0.5 μM) as well as 0.25 mM IBMX (3F protocol) to induce adipogenic environment in beating EBs. 5 μM rosiglitazone (Cayman Chemical Co., MI) and 200 μM indomethacin were added to the 3F protocol to form the 5F protocol. Beating EBs at 30 days of differentiation (30D) were treated with 3F- or 5F-media for 4–5 weeks prior to further investigation. 20 μg/ml 13-HODE (Cayman) was used to activate PPARγ based on published dose-response data[33]. 3 μM GW9662 (Cayman)[22] or 0.5 μM T0070907 (Cayman)[23] was chosen to block 13-HODE action based on their IC50s of specific inhibition of PPARγ activation and assumed competitive antagonism from 13-HODE. N-acetyl-cysteine[34], Ascorbate (1 mM)[34], BIO (Tocris, 1–2.5 μM)[28], and Dickkopf-1 (Invitrogen)[28] were used according to previous publications. All pharmacological agents were purchased from Sigma (St Louis, MO) unless otherwise indicated.

Karyotype analysis and teratoma formation

Karyotype analysis was performed by Cell Line Genetics (Madison, WI). For teratoma formation, we injected ~1×10^6 undifferentiated human iPSCs under the kidney capsule of SCID beige mice (Harlan Laboratories). Tumors were collected 8 weeks after injection for histological sections as well as haematoxylin and eosin staining by the SBMRI Histology Core facility. All animal protocols were approved by the SBMRI Animal Care & Use Committee.

RNA isolation and quantitative RT-PCR

Total RNA from JK#2 & 11 and SW#5, 6, & 7 clones was prepared using mirVana miRNA Isolation Kit (Ambion) from 5–10 EBs or Puromycin-selected CSs after respective treatments. Complementary DNA (cDNA) was synthesized by the QuantiTect RT kit (Qiagen). Quantitative real-time polymerase chain reaction (qRT-PCR) was performed on a Roche LightCycler 480 using the LightCycler 480 SYBR Green I Master kit (Roche) according to protocols recommended by the manufacturer. Real time PCR cycle was 40 cycles (95°C for 20 seconds, 60°C for 30 seconds, and 72°C for 30 seconds). Quantification was carried out by correcting for amplification efficiency of the primer using a standard curve, followed by normalizing transcript levels to the amount of total ubiquitously expressed GAPDH transcripts. Two physical replicates from each of 3 respective sets of experiments were used to construct the histograms in all figures. All qRT-PCR and regular RT-PCR primers are listed in Supplementary Tables 1–2.

Genomic and cDNA sequence analysis

Genomic DNA from three to five colonies of undifferentiated H9 and *PKP2*-iPSCs was collected using QIAamp DSP DNA Mini Kit (Qiagen). Genomic DNA of the *PKP2* gene region was amplified with 5′-TGATGAATAATAGTCTTTGCAGGTGTG (sense) and 5′-

CTGAGGGCTGACCAGATGATCTGG (antisense)[11] by PCR (95°C for 2–3 min; 40 cycles of 95°C for 1 min, 55°C for 1 min, and 72°C for 1 min; followed by 5 min at 72°C). PCR products were directlyused for sequencing with two primers as published previously[11].

For the expressed *PKP2*, cDNA was synthesized with Oligo-dT primer and Superscript III reverse transcriptase (Invitrogen) from Puromycin-purified hESC- or *PKP2* iPSC-CSs. The exon 12–14 regions of *PKP2* cDNA were amplified with two primers: exon 12-F: CTCTCCCTGATTTGGTTTCC and exon 14-R: GTGGCCGGTATCTACTGGTG. PCR products were directly cloned into bacteria by the TOPO TA Cloning kit (Invitrogen) and sequenced using T7 primers at SBMRI DNA analysis facility.

Bisulphite sequencing

Genomic DNA purification from ~2×10^4 cells and bisulphite conversion of purified DNA was performed using the EZ DNA Methylation Direct Kit (Zymo Research) according to the manufacturer's instructions. The *NANOG* promoter region of converted DNA was amplified by PCR using primers: *Nanog*-1F: AGAGATAGGAGGGTAAGTTTTTTTT and *Nanog*-1R: ACTCCCACACAAACTAACTTTTATTC. PCR products were directly cloned into bacteria and sequenced as mentioned above.

Gene microarray analysis

Total RNA was extracted from ~1×10^5 cultured fibroblasts, or 5–10 undifferentiated hESCs or iPSCs. Sample amplification, labelling, and hybridization on Illumina Human HT-12v4 arrays (Illumina, Inc., San Diego) were performed for all arrays using Illumina BeadStations in the SBMRI and Scripps Research Institute Microarray Core facilities according to the manufacturer's instructions (http://www.illumina.com). Quality control of raw data was performed with the GenomeStudio software (Illumina) and analyzed with various software detailed in the Supplementary Information. For the heat map, values across each probe were standardized to have mean 0 and standard deviation (SD) 1, and then plotted on a color scale where green denotes negative SD; black, 0; and red, positive SD. The heat map showed close hierarchical clustering between hESCs and iPSCs based on 5559 genes with at least twofold changes in mRNA expression levels when compared to the average levels of three fibroblast lines.

Lentiviral construction and viral transduction

Wild-type (WT) *PKP2* cDNA was first cloned into pcDNA3.1 plasmid and the Xba1-EcoR1 fragment containing WT *PKP2* cDNA was then sub-cloned into pCDH-CMV-MCS-EF1-GFP lentivector [System Biosciences, Inc. (SBI)]. SBI lenti packaging and concentration kit was used for lentiviral production following manufacturer's instructions. We used the same protocol to generate lentiviruses containing control GFP and pRex1:Blasticidin//αMHC:Puromycin (Addgene).

Undifferentiated mutant *PKP2* iPSCs with αMHC-Puromycin resistance were generated according to the detailed protocol published previously[14,32]. To generate mutant *PKP2* iPSC-CMs with overexpression of control GFP or WT *PKP2*-GFP, we transduced mutant *PKP2* iPSC-CMs (~10,000 cells per well) with 8 μg/ml polybrene and control GFP or WT

PKP2-GFP lentiviruses. At 72 hours after transduction, mutant *PKP2* iPSC-CMs were dissociated and plated into Geltrex (Invitrogen)-coated 96-well plates (~1000 cells per well) for pathogenic induction experiments.

Beta-catenin luciferase Assay

Production of lentiviruses containing 7xTcf-FFluc//SV40-Puro[r] (Addgene) is the same as described above. At 72 hours after transduction, cells were replated at 2000 cells per well for 6 hours, then treated with media containing no BIO or 2.5 μM BIO for 16 hours, and subsequently Luciferase assay was performed with Promega Luciferase assay system (Cat. # PRE4030) according to manufacturer's instructions. BIO treatment was used to assess the efficacy of the Luciferase assay and we used GloMax-96 Microplate Luminometer (Promega) to measure luminescent values.

Immunocytochemistry, TUNEL count, and lipid-laden cardiomyocyte count

We prepared 8 μm cryosections of EBs or CSs, and performed immunostaining according to standard protocols published previously[14]. Primary antibodies used were listed in Supplementary Table 3. Alexa Fluor 488 and Alexa Fluor 594 anti-mouse or anti-rabbit IgG (Invitrogen) were the secondary antibodies used for the fluorescence imaging. Samples were imaged on adeconvolution microscope (Observer.Z1, Zeiss, Germany) using the SlideBook software (Intelligent Imaging Innovations, CA).

TUNEL staining with In Situ Cell Death Detection Kit, TMR Red (Roche) and Nile Red staining (10 μg/ml, Sigma) were conducted during the secondary antibody incubation period according to the manufacturer's instructions. TUNEL and Nile Red staining were co-stained with one cardiac marker (cTnI or αActinin antibodies) so that cardiomyocyte-specific apoptosis and lipid-production could be counted. Cryosections with Nile Red staining were magnified using SlideBook so as to count the number of cardiomyocytes that contained any cytoplasmic, round lipid droplets as the lipid-laden cardiomyocytes. Supplementary Table 4 summarized all clones of each type of iPSCs used for various experiments.

Ca^{2+} imaging and curve fitting

Puromycin-purified CSs were manually dissected to small clusters and clusters with slow beating rates (see Supplementary Fig. 16 for details) with or without pathogenic induction at approximately 60D were loaded with Fura-2 AM (Molecular Probe). Ca^{2+} imaging was conducted with an inverted microscope (IX71, Olympus) and a cooled CCD camera (Hamamatsu, Japan) controlled by SlideBook. The $[Ca^{2+}]_i$ was calculated from fluorescence ratio at 500 nm after excitation at 340 and 380 nm with a LAMBDA DG-4 system (Sutter Instrument) according to the standard method[35]. CSs were externally paced at 1Hz with 8V/8ms stimulus strength, and the relaxation phase of Ca^{2+} signals of the last paced beat was analyzed with the SigmaPlot software (SPSS Inc.) using the Marquardt-Levenberg algorithm to obtain the relaxation time constant (τ) of the best single-exponential curve fit. These CSs were then perfused with extra-cellular DMEM containing 5.8 mM Ca^{2+} (high Ca^{2+} media) for 10 minutes to reach steady-state[14]. The τ after a similar pacing protocol was then obtained for comparison. All experiments were conducted at 37°C with all extracellular

solutions pre-oxygenated with 95% O_2/5% CO_2. More than three sets of experiments were performed to construct Supplementary Fig. 13.

Seahorse Metabolic Assay

We used a Seahorse XF96 Extracellular Flux Analyzer[25] to measure oxygen consumption rate (OCR, pmol/min) and extracellular acidification rate (ECAR, the H^+ production rate, mpH/min) of JK mutant *PKP2* iPSC-CMs and normal hS-iPSC-CMs in XF96 well plates according to Installation and Operation Manual from Seahorse Bioscience (MA, USA). XF assay media contain unbuffered DMEM, 5.5 mM glucose, and 0.5 mM carnitine. We used Etomoxir (ETO, 100 μM), a specific CPT-1 inhibitor, to assess the degree of fatty acid oxidation, and 2-deoxyglucose (2-DG, 50 mM), a blocker of glycolysis and pyruvate oxidation, to assess glucose utilization[36].

Intracellular recording

Standard intracellular recording of action potentials was performed as described previously[14].

Statistical Analysis

Data were presented as the mean ± SEM. Using the StatView/JMP program (SAS institute, Cary, NC), statistical difference was analyzed by an ANOVA procedure with post-hoc Tukey/Kramer test for multiple comparisons and by the unpaired *t*-test for pair-wise comparisons. A difference with a p-value < 0.05 was considered statistically significant and was labelled with an asterisk (*) in all figures.

Supplementary Material

Refer to Web version on PubMed Central for supplementary material.

Acknowledgments

References

1. Takahashi K, et al. Induction of pluripotent stem cells from adult human fibroblasts by defined factors. Cell. 2007; 131:861–872. [PubMed: 18035408]

2. Yu J, et al. Induced pluripotent stem cell lines derived from human somatic cells. Science. 2007; 318:1917–1920. [PubMed: 18029452]

3. Park IH, et al. Disease-specific induced pluripotent stem cells. Cell. 2008; 134:877–886. [PubMed: 18691744]

4. Carvajal-Vergara X, et al. Patient-specific induced pluripotent stem-cell-derived models of LEOPARD syndrome. Nature. 2010; 465:808–12. [PubMed: 20535210]

5. Moretti A, et al. Patient-specific induced pluripotent stem-cell models for long-QT syndrome. N Engl J Med. 2010; 363:1397–1409. [PubMed: 20660394]

6. Itzhaki I, et al. Modelling the long QT syndrome with induced pluripotent stem cells. Nature. 2011; 471:225–9. [PubMed: 21240260]

7. Yazawa M, et al. Using induced pluripotent stem cells to investigate cardiac phenotypes in Timothy syndrome. Nature. 2011; 471:230–4. [PubMed: 21307850]

8. Calkins H, Marcus F. Arrhythmogenic right ventricular cardiomyopathy/dysplasia: an update. Curr Cardiol Rep. 2008; 10:367–75. [PubMed: 18715533]

9. Awad MM, Calkins H, Judge DP. Mechanisms of disease: molecular genetics of arrhythmogenic right ventricular dysplasia/cardiomyopathy. Nat Clin Pract Cardiovasc Med. 2008; 5:258–67. [PubMed: 18382419]

10. Okita K, et al. A more efficient method to generate integration-free human iPS cells. Nat Methods. 2011; 8:409–12. [PubMed: 21460823]

11. Awad MM, et al. Recessive arrhythmogenic right ventricular dysplasia due to novel cryptic splice mutation in PKP2. Hum Mutat. 2006; 27:1157. [PubMed: 17041889]

12. Dalal D, et al. Clinical features of arrhythmogenic right ventricular dysplasia/cardiomyopathy associated with mutations in plakophilin-2. Circulation. 2006; 113:1641–9. [PubMed: 16549640]

13. Garcia-Gras E, et al. Suppression of canonical Wnt/beta-catenin signaling by nuclear plakoglobin recapitulates phenotype of arrhythmogenic right ventricular cardiomyopathy. J Clin Invest. 2006; 116:2012–21. [PubMed: 16823493]

14. Kim C, et al. Non-cardiomyocytes influence the electrophysiological maturation of human embryonic stem cell-derived cardiomyocytes during differentiation. Stem Cells Dev. 2010; 19:783–95. [PubMed: 20001453]

15. Onay-Besikci A. Regulation of cardiac energy metabolism in newborn. Mol Cell Biochem. 2006; 287:1–11. [PubMed: 16670818]

16. Lopaschuk GD, Ussher JR, Folmes CD, Jaswal JS, Stanley WC. Myocardial fatty acid metabolism in health and disease. Physiol Rev. 2010; 90:207–58. [PubMed: 20086077]

17. Ali AT, et al. The relationship between alkaline phosphatase activity and intracellular lipid accumulation in murine 3T3-L1 cells and human preadipocytes. Anal Biochem. 2006; 354:247–254. [PubMed: 16750158]

18. Taura D, et al. Adipogenic differentiation of human induced pluripotent stem cells: comparison with that of human embryonic stem cells. FEBS Lett. 2009; 18:1029–33. [PubMed: 19250937]

19. Gregoire FM, Smas CM, Sul HS. Understanding adipocyte differentiation. Physiol Rev. 1998; 78:783–809. [PubMed: 9674695]

20. Djouadi F, et al. A potential link between peroxisome proliferator-activated receptor signalling and the pathogenesis of arrhythmogenic right ventricular cardiomyopathy. Cardiovasc Res. 2009; 84:83–90. [PubMed: 19497962]

21. Son N, et al. Cardiomyocyte expression of PPARgamma leads to cardiac dysfunction in mice. J Clin Invest. 2007; 117:2791–801. [PubMed: 17823655]

22. Willson TM, Lambert MH, Kliewer SA. Peroxisome proliferator-activated receptor gamma and metabolic disease. Annu Rev Biochem. 2001; 70:341–67. [PubMed: 11395411]

23. Waku, et al. The nuclear receptor PPARγ individually responds to serotonin- and fatty acid-metabolites. EMBO J. 2010; 29:3395–407. [PubMed: 20717101]

24. Scolletta S, Biagioli B. Energetic myocardial metabolism and oxidative stress: let's make them our friends in the fight against heart failure. Biomed Pharmacother. 2010; 64:203–7. [PubMed: 19954925]

25. Ferrick DA, Neilson A, Beeson C. Advances in measuring cellular bioenergetics using extracellular flux. Drug Discov Today. 2008; 13:268–74. [PubMed: 18342804]

26. Neubauer S. The failing heart – An engine out of fuel. N Engl J Med. 2007; 356:1140–51. [PubMed: 17360992]

27. Kléber AG, Rudy Y. Basic mechanisms of cardiac impulse propagation and associated arrhythmias. Physiol Rev. 2004; 84:431–88. [PubMed: 15044680]

28. Qyang Y, et al. The renewal and differentiation of Isl1+ cardiovascular progenitors are controlled by a Wnt/β-Catenin Pathway. Cell Stem Cell. 2007; 1:165–179. [PubMed: 18371348]

29. Cai CL, et al. Isl1 identifies a cardiac progenitor population that proliferates prior to differentiation and contributes a majority of cells to the heart. Dev Cell. 2003; 5:877–889. [PubMed: 14667410]

30. Lombardi R, et al. Genetic fate mapping identifies second heart field progenitor cells as a source of adipocytes in arrhythmogenic right ventricular cardiomyopathy. Circ Res. 2009; 104:1076–84. [PubMed: 19359597]

31. Kattman SJ, et al. Stage-specific optimization of activin/nodal and BMP signaling promotes cardiac differentiation of mouse and human pluripotent stem cell lines. Cell Stem Cell. 2011; 8:228–40. [PubMed: 21295278]

32. Kita-Matsuo H, et al. Lentiviral Vectors and Protocols for Creation of Stable hESC Lines for Fluorescent Tracking and Drug Resistance Selection of Cardiomyocytes. PLoS ONE. 2009; 4:e5046. [PubMed: 19352491]

33. Nagy L, et al. Oxidized LDL regulates macrophage gene expression through ligand activation of PPARgamma. Cell. 1998; 93:229–40. [PubMed: 9568715]

34. Dhalla NS, Elmoselhi AB, Hata T, Makino N. Status of myocardial antioxidants in ischemia-reperfusion injury. Cardiovasc Res. 2000; 47:446–56. [PubMed: 10963718]

35. Grynkiewicz G, Poenie M, Tsien RY. A new generation of Ca2+ indicators with greatly improved fluorescence properties. J Biol Chem. 1985; 260:3440–50. [PubMed: 3838314]

36. http://www.seahorsebio.com/learning/tech-writing.php
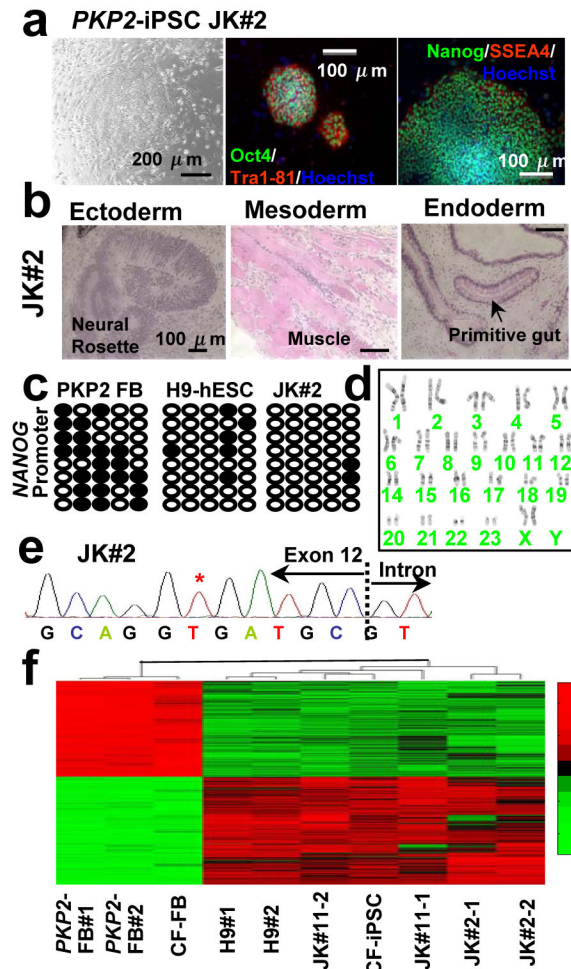
Figure 1. Generation of c.2484C>T *PKP2* mutant iPSCs
a, The JK#2 clone of mutant iPSCs expressed significant levels of pluripotent proteins. **b**, Representative images of cells of three germ layers from teratoma sections. **c**, Bisulphite sequencing analysis of the CpG methylation patterns of *NANOG* promoter regions in mutant *PKP2* fibroblasts (FB), hESCs, and JK#2 clone of iPSCs. **d**, Normal karyotype of JK#2 iPSCs. **e**, Genomic DNA sequencing showed the homozygous c.2484C>T (asterisk) *PKP2* mutations in JK#2 iPSCs. **f**, Analysis of genome-wide mRNA expression profiles (Heat map) of all iPSC lines, normal human FB (CF-FB)-derived CF-iPSC, and H9 hESC lines (see Methods and Supplementary Figs.1–2 for detailed description).
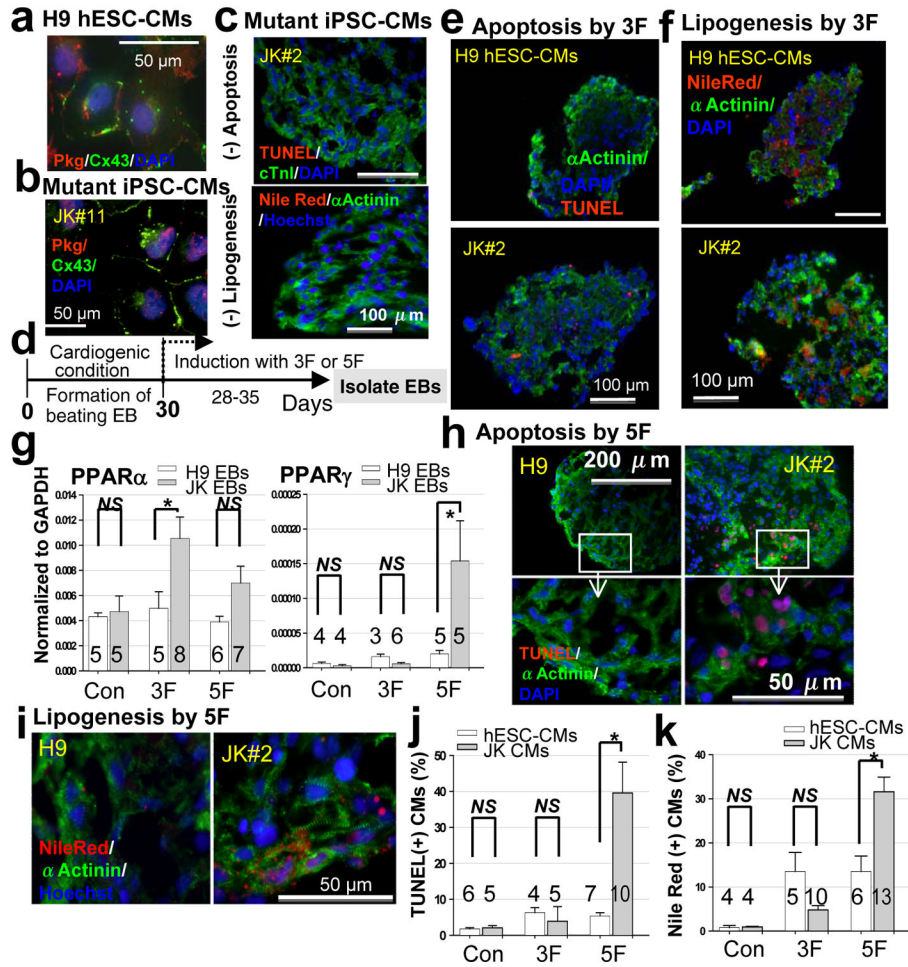
Figure 2. Induction of pathognomonic features of ARVD/C using mutant *PKP2*-iPSCs

a, H9 hESC-CMs showed sarcolemmal connexin 43 (Cx43) and Pkg distribution (red) at both cell membrane and nucleus (DAPI); yet (**b**) Pkg staining in mutant iPSC-CMs is restricted to the nuclei. **c**, At baseline, minimal TUNEL nuclear staining (apoptosis) or Nile-Red labelling (lipogenesis) was found in mutant iPSC-CMs. Pictures with low magnification are used to show the lack of pathologies. **d**, Protocols for lipogenic (3F) and pathogenic (5F) induction. **e**, Minimal apoptosis and (**f**) mild increase of lipid-laden (red) CMs were found after 3F treatment. **g**, Summary of expression levels of PPARα and PPARγ (relative to GAPDH) in beating EBs. PPARα: 4.3±0.3E-3 & 4.7±1.2E-3 at control condition (Con), 5.0±1.3E-3 & 1.1±0.2E-2 after 3F and 3.9±0.5E-3 & 7.0±1.3E-3 after 5F for H9 hESC- and mutant iPSC-CMs, respectively. PPARγ: 6.1±2.1E-6 & 2.9±1.7E-6 at Con, 1.6±0.4E-5 & 5.6±1.8E-6 after 3F and 2.0±0.5E-5 & 1.5±0.6E-4 after 5F. Pictures with higher magnification are used to show significant increase of (**h**) TUNEL-positive and (**i**) lipid-containing CMs after 5F. Summary of (**j**) degrees of apoptosis and (**k**) lipid-laden CMs in beating EBs. The number in each column represents the number of biological replicates tested. Asterisks indicate *p*<0.05 and *NS,* no significant difference by ANOVA. All data are shown as mean±s.e.m.
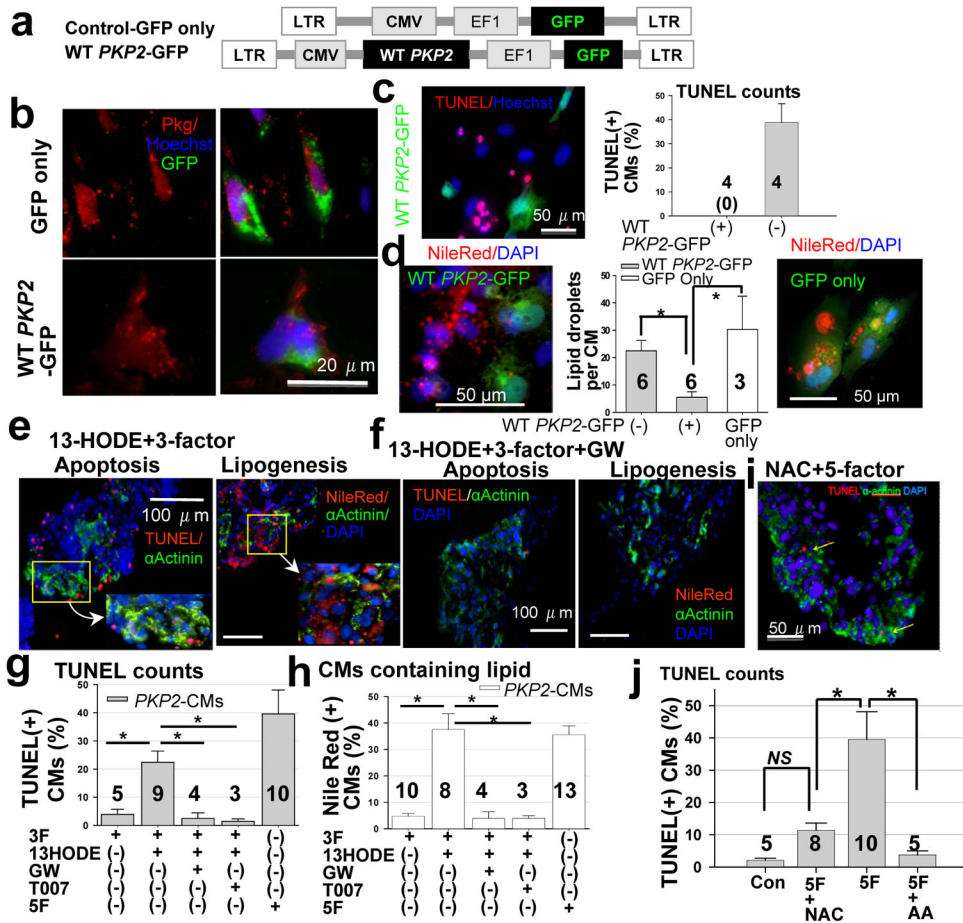
Figure 3. Rescue of pathological features of mutant *PKP2*-iPSC-CMs

a, Diagram of lentiviral vectors used to stably integrate control-GFP or WT-*PKP2*-GFP into mutant iPSC-CMs. **b**, Top panels: Pkg (red) remained restricted to nuclei with control-GFP vectors; yet, bottom panels show Pkg distributed at both cell membrane and nucleus (Hoechst) with WT-*PKP2*-GFP of purified mutant iPSC-CMs. **c**, After 5F and WT *PKP2*-GFP lentiviral infection, TUNEL nuclear staining could only be found in GFP-negative CMs. **d**, Large number of lipid droplets (red) could only be found in WT *PKP2*-GFP-negative (left, 22.5±3.8) or control-GFP-positive CMs (right, 30.3±12.2 lipid droplets per CM), but not in WT *PKP2*-GFP-positive CMs (5.5±2.0 small lipid droplets per CM). **e**, 13-HODE (20 μg/ml) with 3F could replace 5F for pathogenic induction. **f,** 3 μM GW and 0.5 μM T007 (not shown) prevent pathogenic induction by 13-HODE+3F. **g**, Summary of CM apoptotic index and (**h**) degrees of lipogenesis. The percentage of CMs that have TUNEL staining and lipid droplets in mutant iPSC-CMs after treatment with 3F, 13-HODE+3F, 13-HODE+3F+GW, 13-HODE+3F+T007 and 5F (re-plot from Fig. 2j–k) are: 3.9±1.8 & 4.8±1.0%, 22.4±4.0 & 37.5±6.0%, 2.5±2.0 & 3.9±2.5%, 1.5±0.9 & 4.0±1.0% and 39.6±8.5 & 31.6±3.3% respectively. **i**, N-acetyl-cysteine (NAC) prevented CM apoptosis induced by 5F. **j,** The apoptotic index for mutant iPSC-CMs after 5F with 1 mM NAC or ascorbic acid (AA) is 11.4±2.3% and 3.8±1.2%, respectively (versus 2.1±0.6% in control and 39.6±8.5
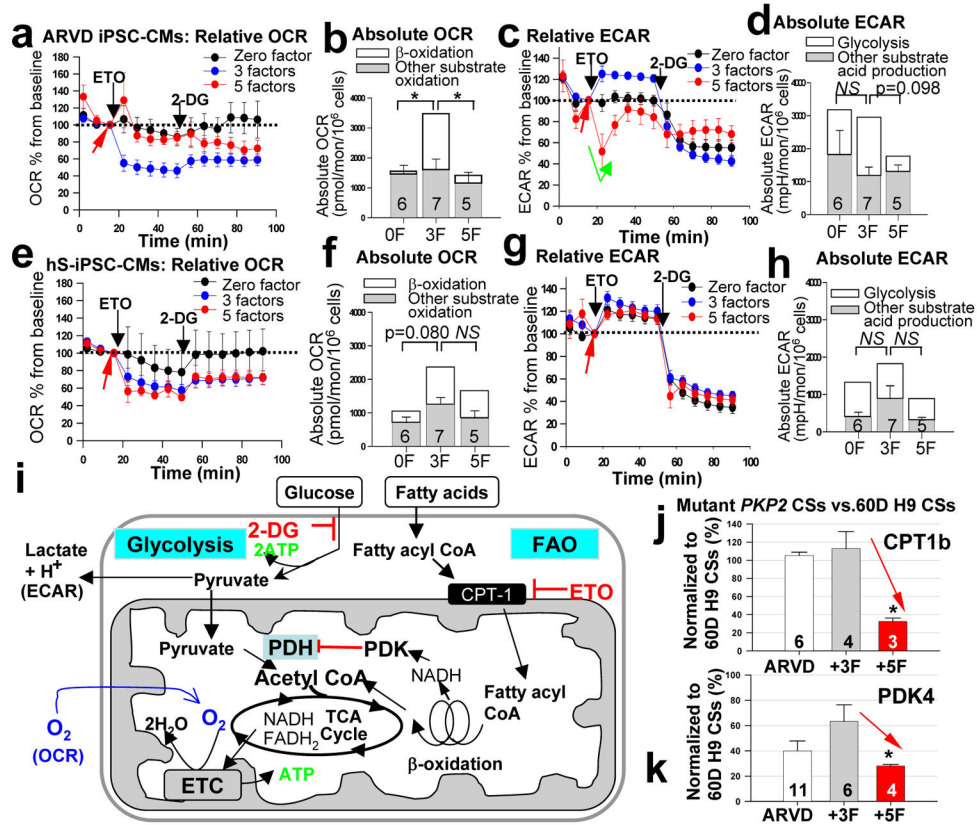
after 5F). The number in each column represents the number of biological replicates tested. Asterisks indicate *p*<0.05 and *NS,* no significant difference by ANOVA.

Figure 4. Metabolic and qRT-PCR assays of glucose and fatty acid utilization of mutant (JK#11 & #2) and normal hS-iPSC-CMs

The Etomoxir (ETO, 100 μM)-blocked component of oxygen consumption rate (OCR) and 2-deoxyglucose (2-DG, 50 mM)-blocked component of extracellular acidification rate (ECAR) represent FAO and glycolysis, respectively. Absolute values of OCR and ECAR are expressed as pmol/min/10^6 cells and mpH/min/10^6 cells, respectively. **a**, Real-time measurement of OCR showed that ETO blocked 14.4±10.2 (0F), 53.9±8.2 (3F) and 15.3±8.5% (5F) of baseline OCR (red arrow) for mutant iPSC-CMs. **b**, ETO-blocked absolute OCR (white boxes) for mutant iPSC-CMs are 85.2±196.6 (0F), 1865.3±383.5 (3F) and 254.5±115.4 (5F). **c**, ECAR measurement after ETO inhibition of β-oxidation showed a rapid ~21% compensatory increase of glycolysis only in the 3F condition (a switch in energy substrates); yet, after 5F, ETO transiently decreased ECAR by ~45% (green arrow) followed by ~28% compensatory increase in ECAR (glycolysis). **d**, 2DG-blocked absolute ECAR (glycolysis) for mutant iPSC-CMs after 0F, 3F or 5F are 1353.0±313.6, 1766.0±579.7 and 457.2±211.0, respectively. Comparable patterns in absolute and relative OCR or ECAR in normal hS-iPSC-CMs (WS#4) are shown in (**e–h**). For normal iPSC-CMs, ETO-blocked FAO after 0F, 3F or 5F are (**e**) (relative) 21.8±24.8%, 42.6±6.6% and 50.5±4.06%; or (**f**) (absolute) 329.4±235.8, 1114.5±316.6 and 807.8±196.4, respectively. 2DG-blocked glycolysis after 0F, 3F or 5F are (**g**) (relative) 65.5±5.3%, 54.9±3.8% and 58.8±4.8%; or (**h**) (absolute) 915.3±270.6, 929.4±314.3 and 556.8±217.9, respectively. Combining data shown in **a–h**, these results support that both normal and mutant iPSC-CMs 1) display embryonic metabolism at the baseline, and 2) show significantly increases FAO

after 3F with ability to switch between FAO and glucose utilization (an adult-like metabolic pattern). Mutant iPSC-CMs after 5F behave like failing cardiomyocytes (also see Supplementary Fig. 8) with pathological glucose-dominant metabolism. **i,** A simple diagram to illustrate substrate utilization pathways in cardiomyocytes. qRT-PCR analysis of Puromycin-purified mutant iPSC-CMs showed that mutant iPSC-CMs displayed significantly decreased expression of (**j**) CPT-1b and (**k**) PDK4 mRNA transcripts when compared to control H9 hESC-CMs after 5F induction, leading to enhanced pyruvate oxidation and decreased FAO, respectively. Please see Supplementary Information for detailed legend of Fig. 4. Single asterisk indicates $p<0.05$ and *NS,* no significant difference by ANOVA. *P* values are shown when unpaired *t*-test was performed.